

UNCERTAINTY ANALYSIS OF MULTICOMPONENT ELASTIC INVERSION OF THIN-LAYERS

Allan Peixoto de Franco ^{1*}, Sérgio Adriano Moura Oliveira ^{1,2} and Fernando Sergio Moraes ²

ABSTRACT. We assessed the effectiveness of seismic inversion in estimating the elastic properties of layers whose thickness represents a fraction of the wavelength. We used an approach that integrates a quantitative study of inversion uncertainties based on the stochastic Bayesian method and sensitivity analysis, considering the full waveform seismic response of the layer model. Three inversion input data combinations PP, PS, and joint PP-PS reflections provide comprehensive information for the analysis. Estimates of V_p , V_s , and the density of thin layers are sensitive to the intensity of the elastic property contrasts and incidence angle coverage. Results show that the elastic parameters of layers as thin as 1/16 of the peak wavelength can be estimated with low uncertainty if the input data contain incidence angles up to 40 degrees for the PP-PS case and up to 55 degrees for the PP case, when the elastic property contrast is not small.

Keywords: stochastic inversion; reflectivity method; sensitivity analysis.

RESUMO. Nós avaliamos a eficácia da inversão sísmica na estimativa das propriedades elásticas de camadas cuja espessura representa uma fração do comprimento de onda. Utilizamos uma abordagem que integra um estudo quantitativo de incertezas de inversão baseado no método estocástico Bayesiano e análise de sensibilidade, considerando a resposta sísmica completa da forma de onda do modelo de camadas. As análises foram realizadas em três combinações de dados de entrada para inversão: PP, PS e reflexões PP-PS conjuntas. As estimativas de V_p , V_s e densidade de camadas finas são sensíveis à intensidade dos contrastes de propriedades elásticas e à cobertura do ângulo de incidência. Os resultados mostram que os parâmetros elásticos de camadas tão finas quanto 1/16 do comprimento de onda de pico podem ser estimados com baixa incerteza se os dados de entrada contiverem ângulos de incidência de até 40 graus para o caso PP-PS e até 55 graus para o caso PP, quando o contraste da propriedade elástica não é pequeno.

Palavras-chave: inversão estocástica; método da refletividade; análise de sensibilidade.

*Corresponding author: Allan Peixoto de Franco

¹Universidade Estadual do Norte Fluminense (UENF), Laboratório de Engenharia de Exploração e Produção de Petróleo (LENEP), Av. Brennand, Imboassica, 27930-480 Macaé, RJ, Brazil – E-mails: allandefranco@gmail.com, moura@lenep.uenf.br, fernando@lenep.uenf.br

²Instituto Nacional de Ciência e Tecnologia em Geofísica do Petróleo (INCT-GP)

INTRODUCTION

Many oil and natural gas reserves occur in geological layers whose thicknesses are below the limit of seismic resolution, making it impossible for the interpreter to discern the top and bottom of such layers. There has been a large amount of effort in establishing the limit of seismic resolution of thin layers (see, e.g., Widess, 1973, 1982; Koefoed, 1981; Kallweit and Wood, 1982; Zeng, 2009). This limit is generally accepted as a quarter of the dominant wavelength in the layer and applies to seismic sections that have undergone conventional processing to approximate zero-offset sections (Kallweit and Wood, 1982). Widess (1973) studies the tuning effect to establish a thickness of one-eighth as the limit of seismic resolution corresponding to the point that top and bottom reflections are completely combined.

The characterization of reservoirs that are below tuning thickness is a challenging task. In particular, the question of how thin a layer can be, and if a person can still reasonably estimate its property by seismic inversion, is not well understood, especially in the case of the elastic inversion of prestack data. This issue becomes complex since it depends on factors such as the noise level in the data and the accuracy of the estimated seismic wavelet.

The elastic seismic response of thin layer reservoirs has been addressed in many studies in the context of AVO analysis, such as Simmons and Backus (1994), Widmaier et al. (1996), Liu and Schmitt (2003) and Rubino & Velis (2011). These works demonstrate that the convolutional model based on primary reflections alone and approximations for the reflection coefficient is unsuitable for studying thin layers. In this case, other modes of propagation that appear in the layer, notably the locally converted waves, can have a first-order influence on the amplitude of the recorded signal, if the incidence angle is not small. This conclusion is confirmed in a physical seismic modeling work by Assis et al. (2017). Although the above referenced works are essentially devoted to modeling the seismic response of thin layers, there are only a few examples when the topic is seismic inversion of thin layers. Rubino and Velis (2009)

propose a specially developed elastic inversion method for thin layers. Their work presents a non-linear inversion in the frequency versus angle domain using simulated annealing, which in addition to primary wave velocity V_p , secondary wave velocity V_s , and density ρ also determines the layer thickness. The authors reported success in resolving sub-tuning layer thicknesses. In another example, Pan et al. (1994) present a target-oriented elastic inversion that under favorable conditions can estimate elastic properties of a layer with thickness down to one-tenth of the wavelength. Such articles are more focused on the inversion algorithm itself than on the understanding of the limitations of seismic elastic inversion related to thin layers.

The seismic data are band-limited, have a limited angle coverage, and are contaminated by noise. As a result, seismic inversion is an ill-posed problem, considering that many different models may explain the data within the error bounds. The linear inversion approach offers an elegant and convenient way to analyze these effects in elastic inversion, since a covariance matrix can be readily obtained by means, for example, of SVD technique (De Haas and Berkhout, 1988; Van Rijssen and Herman, 1991; Jing and Rape, 2004; Khare and Rape, 2007). Another way to deal with ill-posed inverse problems is to use stochastic methods that perform an extensive random or pseudo-random exploration of the model space to test many possible solutions (Sambridge and Mosegaard, 2002). In a stochastic inversion, the model parameters are treated as random variables, and the solution is given by a probability density function (Tarantola, 1987). The advantages of this approach are the nonnecessity to assume a linear relationship between data and model parameters and the possibility of calculation of uncertainty associated with the estimates (Gouveia and Scales, 1997, 1998).

In this work, besides the stochastic inversion approach based on a Bayesian formulation, we use the classical Metropolis algorithm from Monte Carlo Markov Chain (MCMC) methods to sample the posterior probability density function. From these sample values, we get estimators for the elastic parameters, like mean, and measures of uncertainty,

like standard deviations and correlations between the estimated elastic parameters.

We begin this paper describing the modeling procedure used to calculate prestack data (angle gathers) of a thin layer using the reflectivity method. The strategy adopted here consists of analyzing the estimated elastic parameters and uncertainties resulted from several numerical inversion experiments with varying degrees of elastic property contrast, layer thickness, incidence angle coverage, and input data (PP, PS, and PP-PS). We parameterized our inversion model, for all input data, in terms of V_p , V_s , and ρ . We conducted a sensitivity study to analyze how a change in each of these layer parameters influences the seismic response. This analysis provides fundamental information to understand the behavior of the uncertainties.

METHODS

Modeling of the elastic thin layer seismic response

The practical elastic modeling and inversion methods commonly used in the E&P industry assume the subsurface is locally 1D and are based on the convolutional model of only primary reflections that uses approximations for the reflection coefficients in order to explain the amplitudes of the prestack seismic data. However, these approximations assume small contrasts in elastic properties between layers and are not valid for post-critical angles of incidence (Aki & Richards, 2002). Besides this, convolutional elastic modeling also assumes that the seismic response of the Earth contains only primary reflections. For these reasons, AVO analyses based in such approximations should be restricted to angles not greater than 30 degrees, as shown, for example, in the study of Mallick (2007), that compares the prestack wave-equation modeling with the convolutional modeling using exactly Zoeppritz and Aki & Richards approximation. The influence of the local PS converted waves in elastic modeling and inversion for layered media can be found in Hounie & Oliveira (2014).

Here we consider the upgoing P waves and S waves generated by downgoing transient elastic plane P wave at different angles of reflection on a thin layer. These waves are referred to as PP and PS waves (see Fig. 1). In this case, it is important to consider all events generated in the layer, like multiples, transmission effects, and mode conversions of all types, not only primary reflections (see Fig. 2). This occurs because the traveltime difference between these different wave modes is very small in a thin layer case, making the corresponding waveforms indistinguishable from each other for a band-limited seismic pulse and making it impossible to separate them from the primary reflections. The influence of these events in the AVO response becomes more evident as layer thickness decreases, elastic property contrast increases, and incidence angle grows wider, as noted by Simmons and Backus (1994) and more recently by Assis et al. (2017) in a reduced scale physical modeling study.

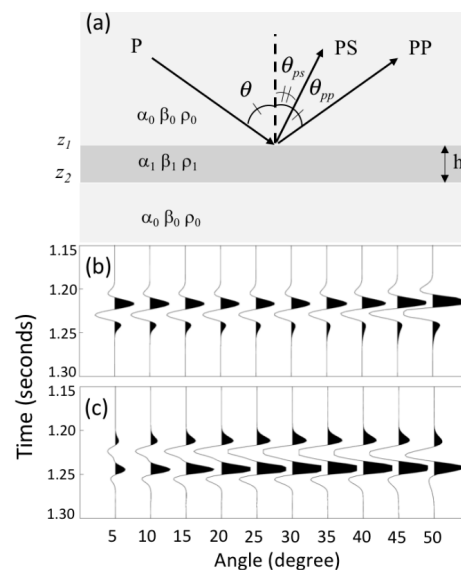


Figure 1 - (a) The single layer model used in the inversion tests (b) the PP angle gather (c) The PS angle gather, both generated for medium contrasts and $h = \lambda/2$.

The reflectivity method (Muller 1985) is used for modeling the seismic response of the thin layer model. Some details about this modeling procedure are given in the appendix. The PP and PS plane wave responses can be given as a function of the ray parameter $p = \sin\theta/\alpha_0$ and the vertical two-way travel time τ by the following inverse Fourier transforms:

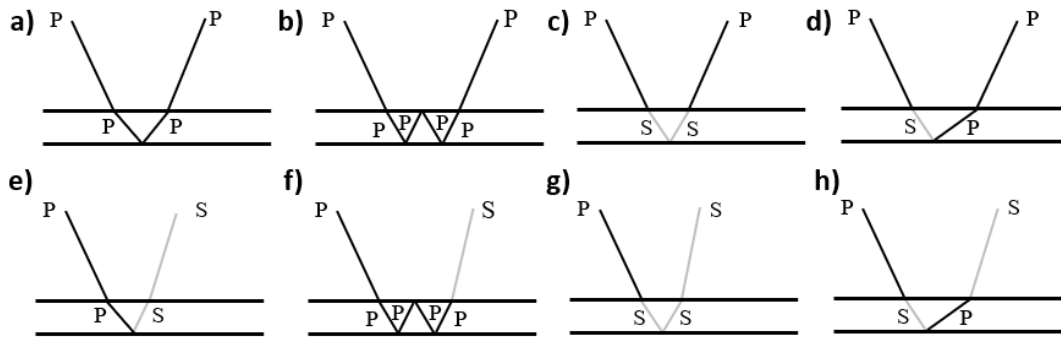


Figure 2 - Representation of PP (a) and PS (e) primaries and some of the expected events that occurs in a single thin layer, like Internal multiple (b, f) and local conversions of PP (c, d) and PS (g, h) waves. These events can influence the response predicted by the conventional AVA inversion that considers only primaries (a, e).

$$s_{pp}(\tau, p) = \frac{1}{2\pi} \int_{-\infty}^{\infty} r_{pp}^0(\omega) e^{-i2k_z^0 z_1} F(\omega) e^{-i\omega\tau} d\omega \quad (1)$$

$$s_{ps}(\tau, p) = \frac{1}{2\pi} \int_{-\infty}^{\infty} r_{ps}^0(\omega) e^{-i(k_z^0 + \eta_z^0) z_1} F(\omega) e^{-i\omega\tau} d\omega \quad (2)$$

Where z_1 is the depth of the top interface, α_0 and β_0 are respectively the P wave and S wave velocity of the upper semi space. The frequency domain function of the seismic pulse is $F(\omega)$; r_{pp}^0 is the PP reflectivity; and r_{ps}^0 is the PS reflectivity. They are elements of the reflectivity matrix (A2) that can be obtained by equation (A5). The vertical wavenumbers for P and S waves in the upper semi space are, respectively $k_z^0 = \omega \sqrt{(\frac{1}{\alpha_0})^2 - p^2}$; and $\eta_z^0 = \omega \sqrt{(\frac{1}{\beta_0})^2 - p^2}$.

In practical applications, the input seismic data for prestack inversion are sorted by offset or incidence angle. Due to this, the PP and PS plane wave seismograms are submitted to τ - p NMO correction (Diebold and Stoffa, 1981) and then transformed from ray parameter domain to incidence angle domain using a simple mapping procedure based on Snell law for elastic waves: $p = \sin \theta_{pp} / \alpha_0 = \sin \theta_{ps} / \beta_0$, where $\theta_{pp} = \theta$ is the PP reflection angle and θ_{ps} is the PS conversion angle. This kind of data is known as angle gather seismogram. The data in Figures 1b and 1c represent PP and PS angle gathers (respectively) computed using a single layer model with moderate contrast in elastic properties (see Table 1). For the computation of the seismic data, we use the second derivative of the Gaussian function

as the seismic pulse, and the layer thickness of 25 meters, which corresponds to $1/4\lambda$, where λ is the wavelength related to the peak frequency of P wave in the layer. Note that the seismic response results from the summation of all wave modes represented in Figure (2a-d) for PP waves and in Figure (2e-h) for PS waves.

Bayesian Inversion by MCMC

The goal of the Bayesian inversion is to obtain the probability density function that describes the parameters of the medium. This function is known as the posterior probability distribution, which is represented by

$$P(\mathbf{m}|\mathbf{d}) = kP(\mathbf{d}|\mathbf{m})P(\mathbf{m}) \quad (3)$$

where $P(\mathbf{d}|\mathbf{m})$ is the distribution of the observed data \mathbf{d} given a model \mathbf{m} , also known as the likelihood function. $P(\mathbf{m})$ is the prior distribution of \mathbf{m} and k is a normalization constant that ensures that $\int P(\mathbf{m}|\mathbf{d})d\mathbf{m} = 1$. For the likelihood we chose a Gaussian distribution, given by

$$P(\mathbf{d}|\mathbf{m}) = \frac{1}{\sqrt{(2\pi)^N |\det(\mathbf{C}_e)|}} \exp \left[-\frac{1}{2} (\mathbf{d} - G(\mathbf{m}))^T (\mathbf{C}_e)^{-1} (\mathbf{d} - G(\mathbf{m})) \right] \quad (4)$$

where, for the PP case, $\mathbf{d} = [\mathbf{d}_{pp}]$; for the PS case, $\mathbf{d} = [\mathbf{d}_{ps}]$; for the PP-PS case, $\mathbf{d} = [\mathbf{d}_{pp}, \mathbf{d}_{ps}]$; and \mathbf{d}_{pp} and \mathbf{d}_{ps} represent the vectors of PP and PS data, respectively. The model parameter is represented by \mathbf{m} , G is the forward modeling operator and \mathbf{C}_e is the covariance matrix of the error between the observed and modeled data $\mathbf{e} = \mathbf{d} - G(\mathbf{m})$, in which, in our case, is a simple diagonal matrix that represents the variance of a

white noise. We choose a joint uniform density function for the prior distribution. This means that for a given parameter m_j we have that

$$P(m_j) = \begin{cases} \frac{1}{\Delta m_j} & \text{if } |m_j - \hat{m}_j| \leq \frac{\Delta m_j}{2} \\ 0 & \text{if } |m_j - \hat{m}_j| > \frac{\Delta m_j}{2} \end{cases}, \text{ for } j=1, \dots, M \quad (5)$$

The central interval value is \hat{m}_j and Δm_j is $m_j^{\max} - m_j^{\min}$, the difference between maximum and minimum parameter values. Assuming that the parameters are independent, the joint prior distribution can be written as

$$P(\mathbf{m}) = \prod_{j=1}^M P(m_j) \quad (6)$$

$P(\mathbf{m})$ implies little prior information about the model parameters, except for the interval that the model parameters can vary. This form is suitable to let the inversion results rely on the seismic data alone. Due to the nonlinearity of $G(\mathbf{m})$, the posterior is generally non-Gaussian. However, if the degree of nonlinearity of the problem is not very high, this probability function is not far from a truncated Gaussian.

We use the classical Metropolis algorithm (Metropolis et al., 1953; Hastings, 1970) from MCMC methods to sample the posterior distribution. This method can be summarized by two cycles; the first is the exploration step when a proposed model \mathbf{m}_p is drawn from a current model \mathbf{m}_c using a proposal distribution. In the second step, this proposed model is accepted or rejected according to the following rule:

- Accept \mathbf{m}_p if $P(\mathbf{d}|\mathbf{m}_p) \geq P(\mathbf{d}|\mathbf{m}_c)$.
- If $P(\mathbf{d}|\mathbf{m}_p) < P(\mathbf{d}|\mathbf{m}_c)$ accept \mathbf{m}_p , with

$$\text{probability } \frac{P(\mathbf{d} | \mathbf{m}_p)}{P(\mathbf{d} | \mathbf{m}_c)}.$$

It can be shown that after many cycles, the statistics of the accepted model set corresponds to that of the posterior distribution. Consequently, the mean of the j^{th} model parameter can be calculated by

$$\bar{m}_j = \sum_{n=1}^N \frac{m_j^n}{N} \quad (7)$$

and the standard deviation by

$$\sigma_j = \sqrt{\frac{\sum_{n=1}^N (m_j^n - \bar{m}_j)^2}{N}} \quad (8)$$

where m_j^n corresponds to the j^{th} model parameter generated at the n^{th} simulation. The correlations between two parameters can be obtained using the Pearson formula

$$c_{ij} = \frac{\sum_{n=1}^N (m_i^n - \bar{m}_i)(m_j^n - \bar{m}_j)}{\sqrt{\sum_{n=1}^N (m_i^n - \bar{m}_i)^2} \sqrt{\sum_{n=1}^N (m_j^n - \bar{m}_j)^2}} \quad (9)$$

where c_{ij} is the correlation between m_i and m_j . The values for this coefficient vary between -1 and 1. To facilitate our analysis, we assume that $|c_{ij}| > 0.7$ indicates a strong linear correlation between m_i and m_j , $0.5 < |c_{ij}| < 0.7$ indicates a moderate linear correlation and $|c_{ij}| < 0.5$ indicates a weak correlation. It can be demonstrated that

$$c_{i,j} = \frac{\text{cov}(m_i, m_j)}{\sigma_i \sigma_j} \quad (10)$$

where $\text{cov}(m_i, m_j)$ is the covariance between m_i and m_j . A parameter is well estimated when its standard deviation and also its correlations to others parameters are small. A high correlation between two parameters means that the posterior probability function sees them as having some degree of linear dependence that can give rise to parameter crosstalk, influencing estimation and uncertainty analysis of each other.

RESULTS

Thin-Layer Uncertainties Estimation Experiment

The first inversion experiment is related to the single-layer model schematically represented in Figure 1. We assume that the parameters of the background media are known, making this as a problem of only three parameters: P wave velocity V_p , S wave velocity V_s , and density ρ . This experiment investigates the PP, PS, and PP-PS inversion sensitivity to the contrast degree between the elastic parameters of the layer and

the background media and the thickness of the layer. The inversions are also tested for the angle range of the input data.

The target data for the tests are generated by keeping the layer parameters constant while letting the background medium vary to create the low, medium, and strong contrast cases (see Table 1). Layer thickness is set to different values of $h = \lambda/2$, $h = \lambda/4$, $h = \lambda/8$ and $h = \lambda/16$, according to the wavelength λ of the P wave with peak frequency $f_p = 25$ Hz, so that $\lambda = \alpha_1/f_p$ with α_1 representing the P wave velocity of the layer (see Fig. 1). We choose to set the model parameter values that are representative of a reservoir with positive impedance contrast. Inversion is performed considering the use of three alternative incidence angle ranges of 0-25°, 0-40° and 0-55°. Each inversion test estimates the P wave velocity, S wave velocity, the density of the layer (using the mean as estimator), and its associated standard deviations and correlations.

The wavelet estimation is a well-covered subject in the literature, with approaches that go from a Bayesian estimation (Buland & Omre, 2003) through a spectral method like the spectrum-shaping proposed by Rosa & Ulrych (1991) or the log-spectrum-averaging method proposed by Van der Baan (2008). Since our analysis is based on synthetic data, we assume that the seismic wavelet and the layer thickness are known parameters.

Table 1 – The layer parameters for weak, medium, and high contrast cases.

Parameters	V_p (m/s)	V_s (m/s)	ρ (kg/m ³)
Layer	3500	1750	2450
Background Media (low contrast)	3200	1600	2400
Background Media (medium contrast)	2800	1400	2350
Background Media (strong contrast)	2300	1150	2300

Figure 3 shows two plots of the RMS error between observed and calculated data versus the iteration number for four different runs of the MCMC inversion using respectively (a) PP and (b) PS data. The number of iterations is set to 2000, but the statistics of the posterior distribution is derived from the last 1500 iterations and considering not one but many runs, each one beginning from a different point in the model space, as suggested by Gelman et al. (2013). The data variance is set to 10% of the data maximum amplitude, which represents a moderate noise level. The MCMC method converged with an average acceptance rate of 40%.

The information regarding inversion with PP data is summarized in Figure 4. In this plot, the height of the rectangles indicates the mean obtained for the parameters, while the black vertical bars represent its standard deviations. The shade of gray of the rectangles indicates the thickness of the layer grading from thick (dark gray) to thin (white). The dashed horizontal line represents the true values for V_p , V_s , and ρ . Similar plots are displayed for PS inversion (Fig. 5) and the joint PP-PS inversion (Fig. 6).

By observing the results of the PP inversion (Fig. 4), we note that the standard deviation associated with the estimative of V_p , ρ and V_s increases as the layer becomes thinner. The standard deviation associated with the estimates of V_p and V_s decreases as the input angle range increases; however, this tendency is not clear for ρ . Among the three parameters, V_p has the lowest relative standard deviations and V_s the greatest one. Except for the $\lambda/16$ layer, V_p and ρ are estimated with a standard deviation below 10% of the true value when varying the angle coverage and contrast. It is possible to estimate the three parameters of the $\lambda/16$ layer with a small standard deviation, but it requires an incidence angle range of 0-55°.

The results of PS inversion (Fig. 5) show that, among the three parameters, V_s is the one with the lowest relative standard deviations. Except for the $\lambda/16$ layer case, V_s can be

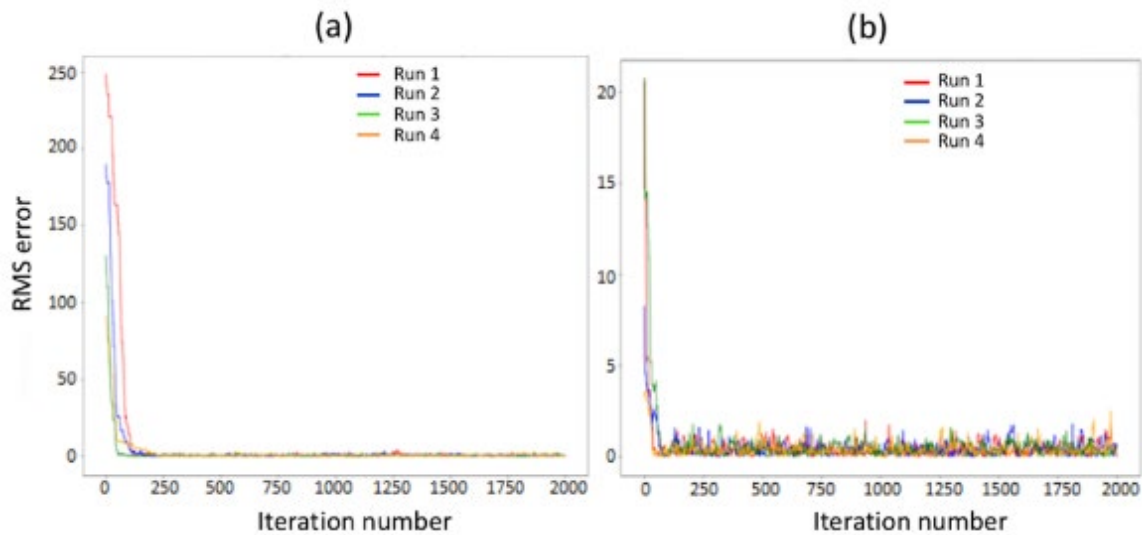


Figure 3 - RMS error between observed and calculated data versus the iteration number for four different runs of the MCMC inversion using the medium contrast model and input data of (a) PP and (b) PS data. The incidence angle range is $0-55^\circ$ and layer thickness is $h=\lambda/4$.

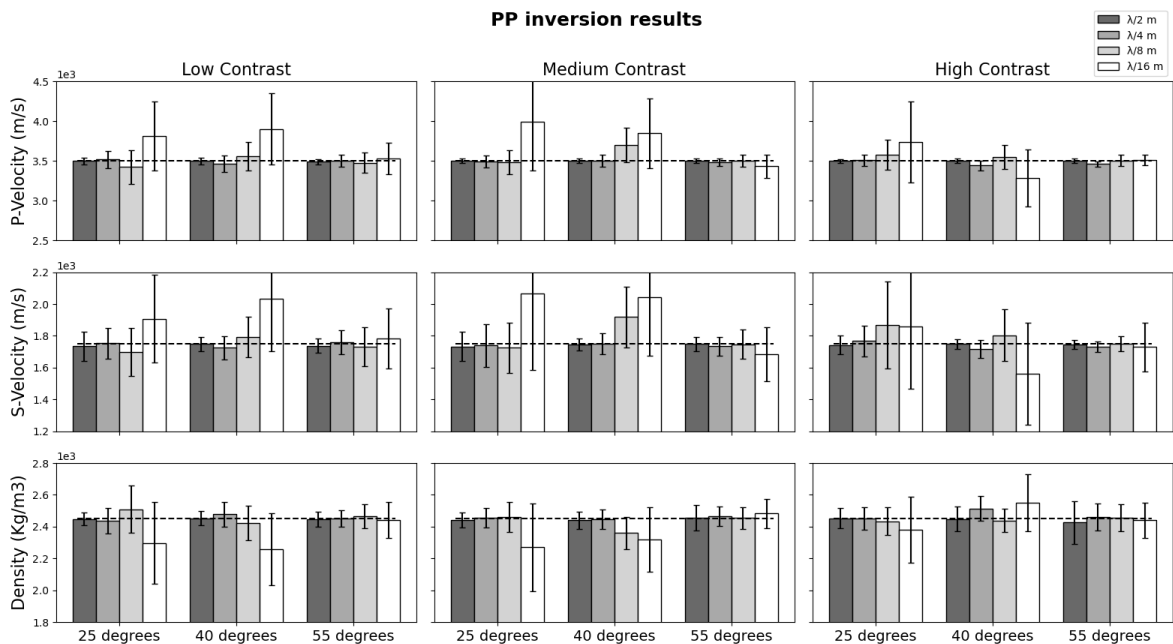


Figure 4 - Results for all PP inversion tests for the single-layer model. The height of the rectangles indicates the mean obtained for the parameters, the black vertical bars represent the corresponding standard deviations, the shade of gray of the rectangles indicates the thickness of the layer, and the dashed horizontal line represents the true values for V_p , V_s and ρ .

estimated with a standard deviation below 10%, while V_p and ρ could be well estimated only for the cases of medium and high contrast and with input angle range exceeding 25° . Note that the property contrast degree affects much more the PS inversion results than that of the PP inversion, especially for V_p and ρ . Interestingly in PS inversion, V_p can be well estimated for layer thicknesses of $\lambda/2$ and $\lambda/4$, but not for other cases with thinner layers. In the PP-PS joint

inversion (Fig. 6), we highlight that the standard deviations associated with the estimative of the three parameters are the smallest for practically all cases, and V_s estimates have the most remarkable improvements in uncertainty (standard deviation) reduction.

The values found for the correlation between the parameters are shown by a color scale scheme where dark blue indicates a strong negative correlation and dark red indicates a

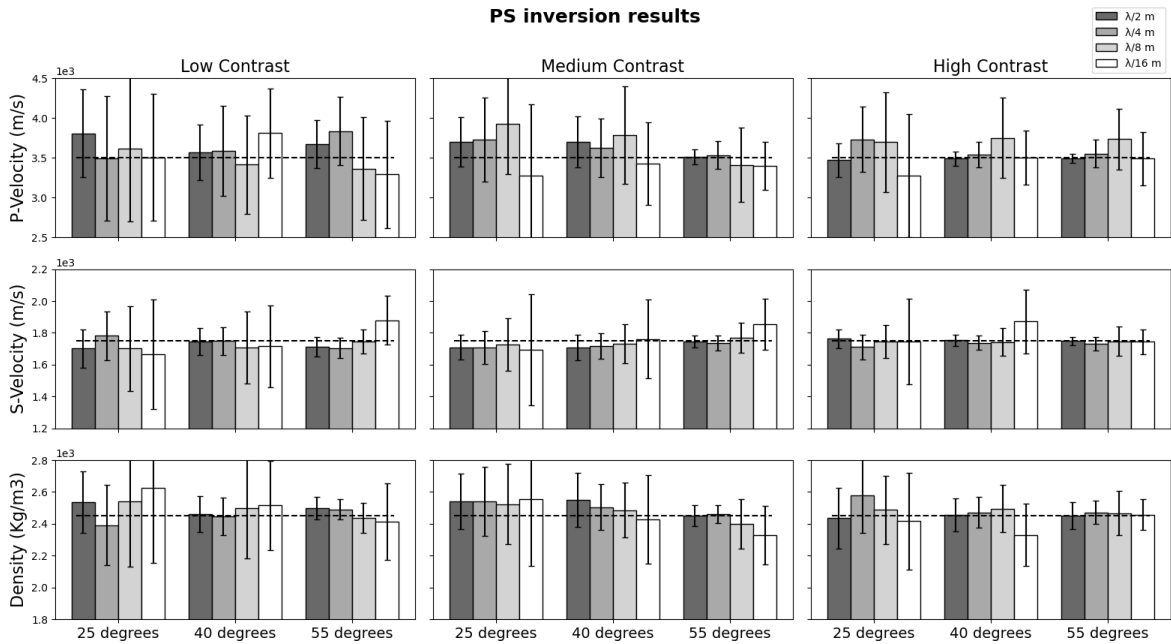


Figure 5 - Results for all PS inversion tests for the single layer model. The height of the rectangles indicates the mean obtained for the parameters, the black vertical bars represent its standard deviations, the shade of gray of the rectangles indicates the thickness of the layer, and the interrupted line represents the true values for V_p , V_s and ρ .

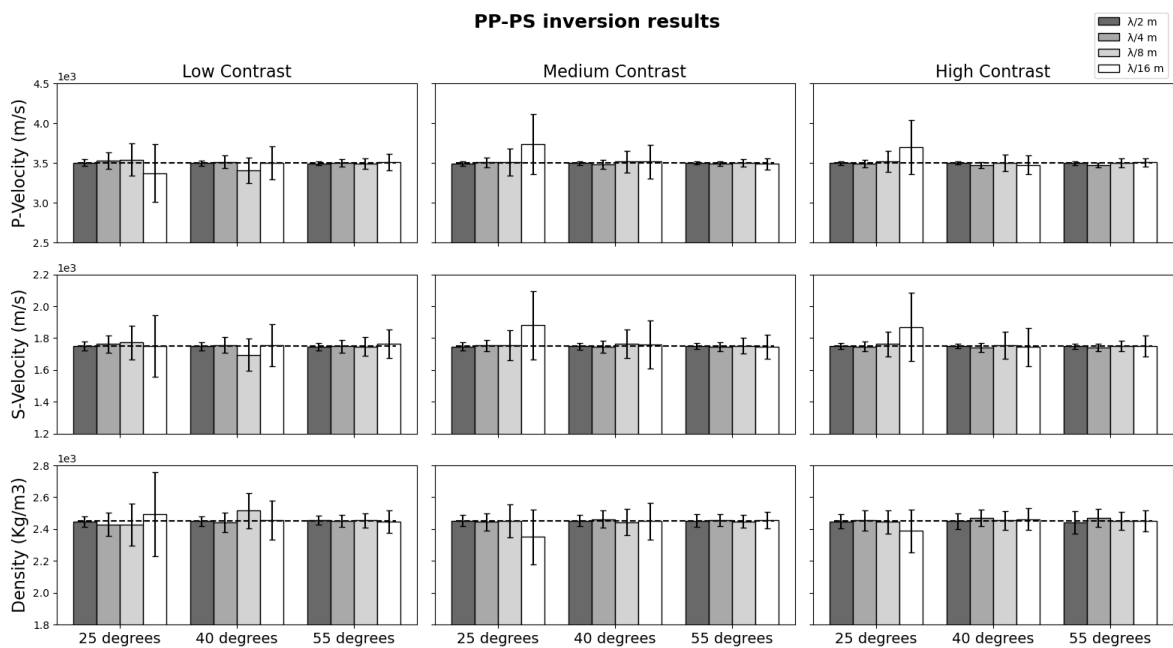


Figure 6 - Results for all PP-PS inversion tests for the single layer model. The height of the rectangles indicates the mean obtained for the parameters, the black vertical bars represent its standard deviations, the shade of gray of the rectangles indicates the thickness of the layer and the interrupted line represents the true values for V_p , V_s and ρ .

strong positive correlation (see Figs. 7, 8, and 9). The analysis of these results shows a well-defined generalized trend of increasing parameter correlation in PP and PP-PS inversions as the contrast and layer thickness decrease. Concerning the angle range in PP, PS and PP-PS inversions, there is no clear correlation tendency.

For some pairs of parameters, the correlation increases (or decreases) when the angle range goes from 0-20° to 0-40°, but then, correspondingly, decreases (or increases) back again when going from 0-40° to 0-55°. For the PS inversion, the parameter correlations are more erratic than in the previous cases. However, it is

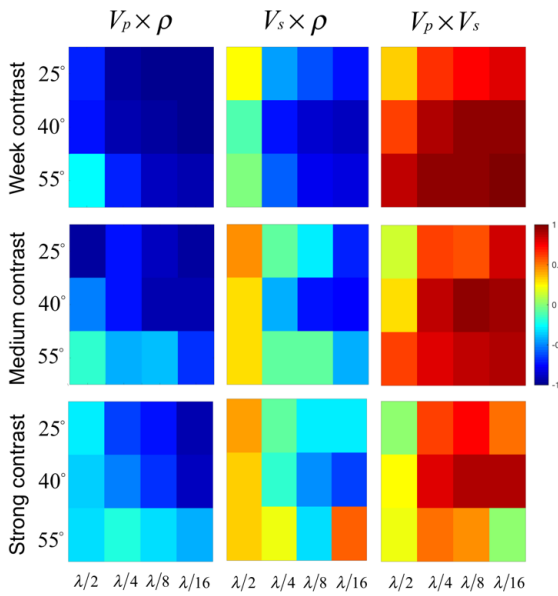


Figure 7 - The correlation between elastic parameters for the PP inversion of a single layer model. The first column refers to $V_p \times \rho$, the second to $V_s \times \rho$, and the third to $V_p \times V_s$.

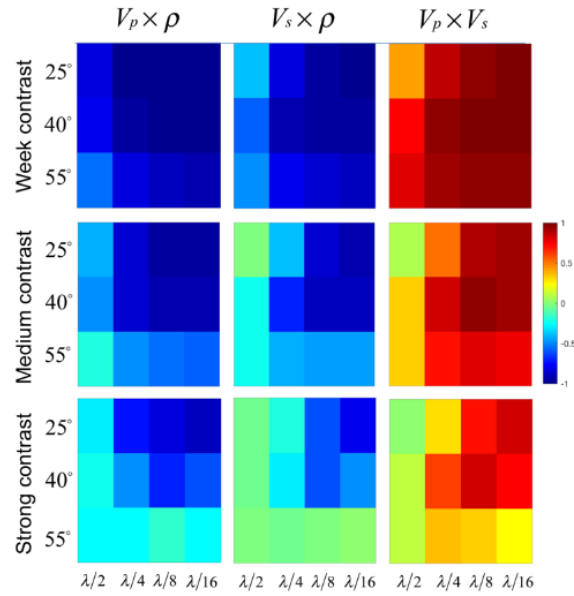


Figure 9 - The correlation between elastic parameters for the PP-PS inversion of a single layer model. The first column refers to $V_p \times \rho$, the second to $V_s \times \rho$, and the third to $V_p \times V_s$.

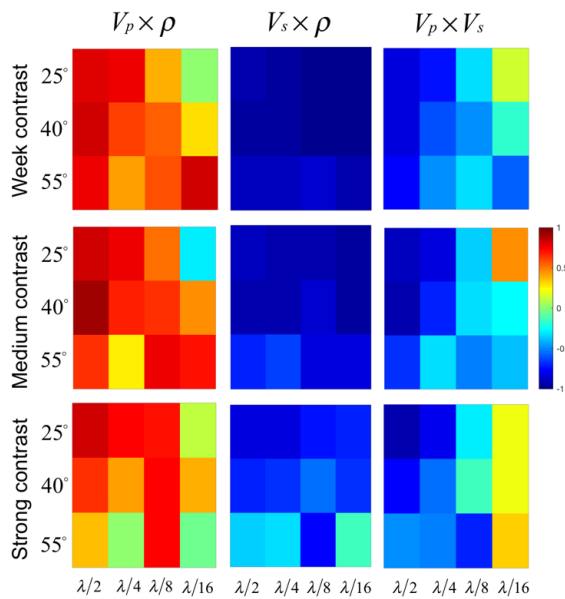


Figure 8 - The correlation between elastic parameters for the PS inversion of a single layer model. The first column refers to $V_p \times \rho$, the second to $V_s \times \rho$, and the third to $V_p \times V_s$.

possible to note that the parameters are also less correlated when the contrast in elastic properties is strong. In PP and PP-PS inversions, V_p - ρ are highly correlated, whereas in PS inversion, high correlations are associated with parameters V_s - ρ . Overall, the behavior of the correlations between the parameters is essentially the same for the PP and PP-PS inversion.

AVA sensitivity curves

This section presents sensitivity AVA curves based on differential seismograms obtained by perturbing the parameter values in the thin layer. This numerical approach is motivated by the complexity of the problem that makes rigorous mathematical analysis difficult to interpret unless severe simplifications are introduced in wave propagation formulation. The differential seismograms make it possible to visualize how data sensitivity to changes in a given parameter vary as a function of the angle of incidence. Following the approach of Oliveira et al. (2018), we can compute the differential seismogram for V_p , which using first-order approximation is given by

$$\frac{ds_{pp}}{dV_p} = \frac{s_{pp}(V_p + \Delta V_p) - s_{pp}(V_p)}{\Delta V_p} \quad (11)$$

The PP and PS differential seismograms obtained for the single-layer model with medium contrasts and $h=\lambda/4$ are shown in Figures 10 and 11, respectively. An AVA sensitivity curve can be derived by picking the amplitudes along the two-way travel time of the top interface of the layer (dashed lines). Each curve represents the rate of change of the amplitude to parameter

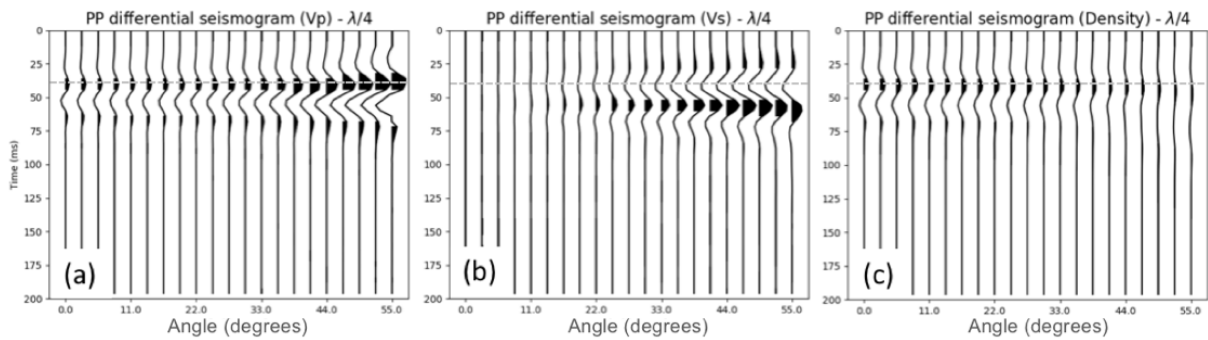


Figure 10 - The PP differential seismograms obtained for the single layer model with medium contrasts and $h = \lambda/4$ for perturbation of (a) V_p (b) V_s , and (c) ρ .

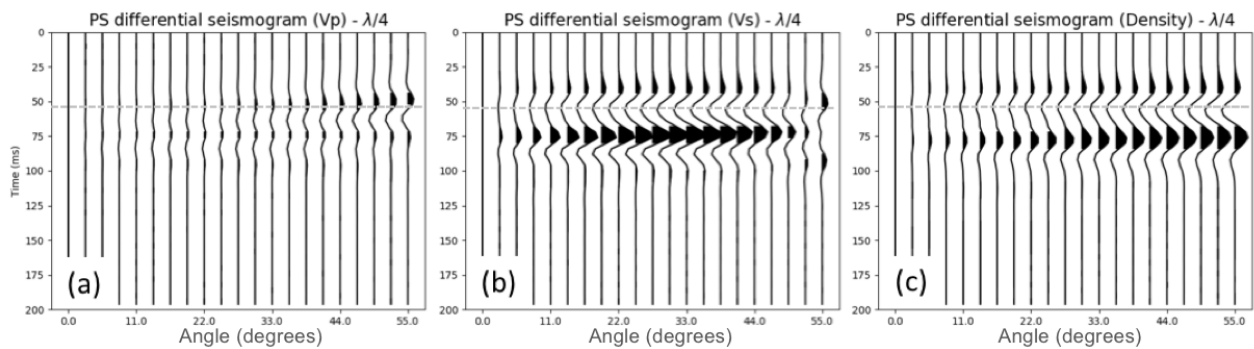


Figure 11 - The PS differential seismograms obtained for the single-layer model with medium contrasts and $h = \lambda/4$ for perturbation of (a) V_p (b) V_s , and (c) ρ .

perturbations as a function of angle, as exhibited in Figure 12 for the PP data and Figure 13 for the PS data. For these examples, we perturb the values of the parameters given in Table 1, using $\Delta V_p = 10 \text{ m/s}$, $\Delta V_s = 10 \text{ m/s}$, and $\Delta \rho = 10 \text{ kg/m}^3$.

We highlight the following facts from these curves: the PP data have very small sensitivity to V_s in the $0\text{-}25^\circ$ angle range. The sensitivity of the PP data with respect to density decreases with angle and becomes very small for angles beyond 40° . The sensitivity of the PP data increases (in absolute value) with the angle for V_p and V_s in the low and medium contrast cases. The AVA sensitivity curves of the PP data with respect to V_p and density are very close to each other for small angles.

The sensitivity of the PS data with respect to density always increases with the incidence angle. The PS data sensitivity with respect to the V_s parameter increases until it reaches the maximum value between 30 and 40 degrees, then it decreases. The PS data are practically insensitive to the variation of the V_p parameter in the small contrast case. However, PS data do have sensitivity to V_p perturbations for the

medium and strong contrast cases if the incidence angle is greater than 30° .

DISCUSSION

The sensitivity analysis proved to be particularly useful to provide a qualitative understanding of the elastic parameter uncertainties related to input data and inversion target features. Overall, the magnitude of the sensitivity curve is related to the standard deviation of the estimate of a given parameter. This connection occurs once the inversion manages to estimate parameters whose data have small sensitive to it. This fact explains the high standard deviations associated with V_s estimates in the PP inversion and V_p estimates in the PS inversion when the input angle range is restricted to $0\text{-}25^\circ$. Low sensitivity also explains why, in the PP inversion, the standard deviation associated with density does not decrease as the incidence angle increases because the density sensitivity curve decreases with the incidence angle, thus adding little additional information at higher angles (see Fig. 12).

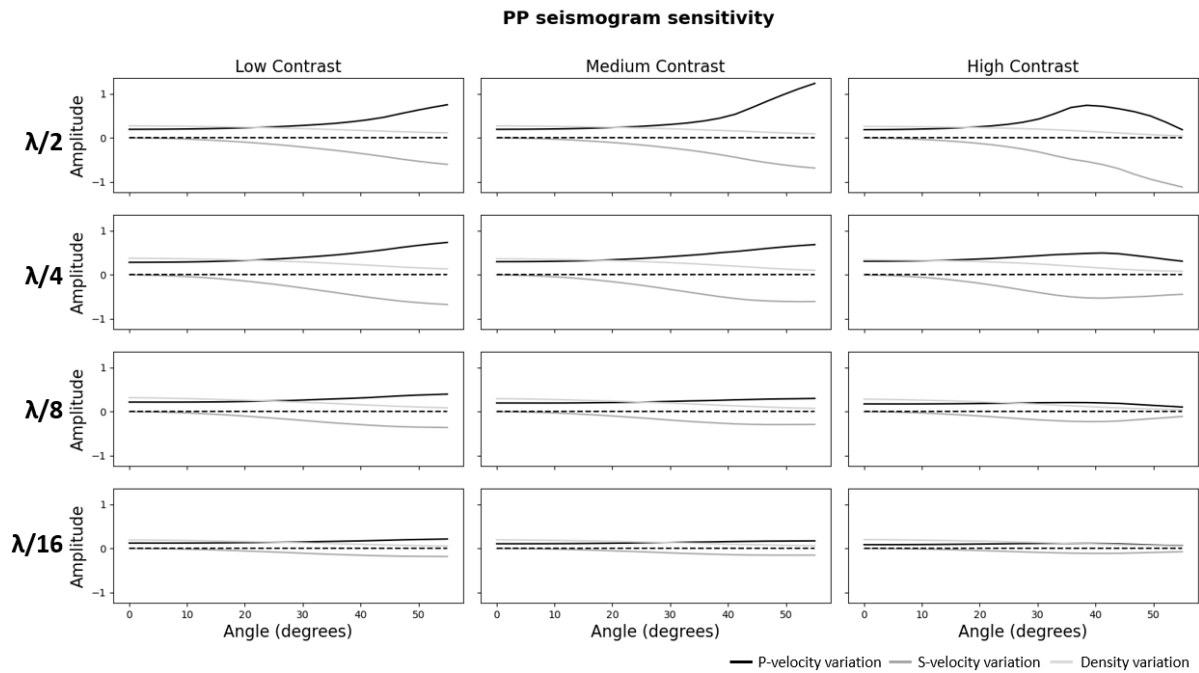


Figure 12 - AVA sensitivity curves derived from PP differential seismograms that were calculated using different thicknesses for the target layer (from $\lambda/2$ to $\lambda/16$) and different contrasts, varying the angle coverage from 0-55°.

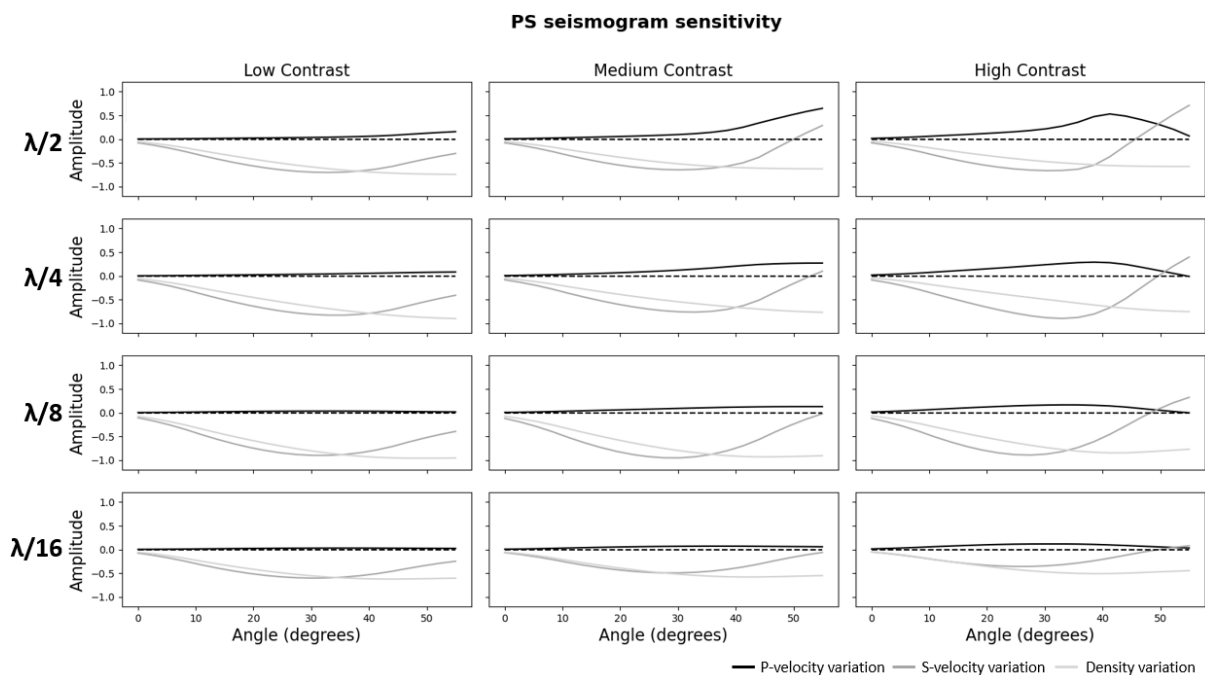


Figure 13 - AVA sensitivity curves derived from PS differential seismograms that were calculated using different thickness for the target layer (from $\lambda/2$ to $\lambda/16$) and different contrasts, varying the angle coverage from 0-55°.

The similarity of two parameter sensitivities affects the correlation between them. That is, if for a given angle range the sensitivities of two parameters are close together (same sign and magnitude), parameter estimates tend to be negatively correlated because decreasing one or increasing the other changes the seismic

response in the same way, as an example of V_p and ρ for small angles in the PP case or V_s and ρ in the PS case (see Figs. 12 and 13). If such curves have similar magnitudes and different signals in the given angle range, the estimate of the parameters tend to be positively correlated, as an example of V_p and V_s in PP case for weak and

moderate contrast and input angle range of 0-40° and 0-50° (see figures). We observe that the sensitivity of the data with all elastic parameters decreases as the layer thickness decreases. The sensitivity curves of all parameters tend to become close to each other as the layer thickness decreases. This explains why both the standard deviation and correlations increase as the layer becomes progressively thinner.

An interesting fact that deserves attention is that the PS data may have a considerable sensitivity to V_p changes. This happens in the strong contrast case, and incidence angles greater than 25°, and also in the medium contrast case, and incidence angle greater than 40°, for layers with thickness greater than $\lambda/8$ (see Fig. 13). For these particular cases, it is possible to estimate V_p from PS data inversion with a small standard deviation. Analyses based on linear AVA approximations cannot reach the same conclusion once the approximated R_{ps} reflection coefficient is independent of ΔV_p (Aki and Richards, 2002). We again recall that the linear AVA approximations, although widely used in practical applications, are valid only for small contrasts between elastic parameters and, since the wave conversion modes influence the primary response for thin layers, these approximations are also only valid for thick layers, which is consistent with our findings described above (see for example, Jing and Rape, 2004). In general case, the PS inversion produces estimates with a very high standard deviation for V_p and ρ , which makes this data inappropriate to be used for elastic inversion of thin layers. However, our analyses demonstrated that the inclusion of PS data in the joint PP-PS inversion for thin layers has a clear impact on decreasing the standard deviations of the estimates of all parameters, especially for V_s that presents a remarkable improvement. The PS data are important to cover the lack of sensitivity of the PP data with respect to V_s , at short angles, and with respect to density, for higher angles.

As we showed in our results, we can resolve parameters corresponding to ultra-thin layers whose thicknesses are below the usual seismic

resolution of $\lambda/4$ dictated by the Rayleigh criteria and even by the Widess criteria of $\lambda/8$. Indeed, the resolution gain obtained by seismic inversion is well known in the literature, as demonstrated by Hill (2005) and Penna & Lupinacci (2021) that exposed the seismic inversion to impedance can provide accurate estimate of thickness below the tuning effect. In our results, we show that the resolution gain provided by an elastic inversion is also influenced by the angle coverage of the input data.

CONCLUSIONS

This article corroborates the conclusions of previous studies of Pan et al. (1994) and Rubino and Velis (2009) which established that it is possible to estimate the elastic properties of very thin layers via elastic inversion. However, a detailed investigation was made here to know under what conditions a given elastic parameter of a thin layer can be reliably estimated, taking into consideration factors as angle coverage of the input data, contrast between elastic parameters and data type (PP, PS and PP-PS). The conclusions reached here were based on the uncertainties of the estimates of the elastic parameters using the stochastic Bayesian MCMC approach for inversion, where the full waveform response of the thin layer was considered, and also on a sensitivity analysis. The main results of this work are summarized below.

To invert V_p , V_s and density for thin layers with thickness between $\lambda/2$ and $\lambda/4$ using conventional PP data, higher angles are essential to decouple V_p from density and to resolve for V_s , in view of the low data sensitivity at small angles. So, it is recommended to use angles up to 40 degrees. For that same thickness range, the elastic parameters can be inverted with low standard deviation from PP-PS data using only angles up to 25 degrees. However, the correlation between V_p and density is still high for small angles in the PP-PS data, especially for thin layers with low contrasts. The uncertainty (especially the correlation between parameters) becomes smaller for both PP and PP-PS cases as the elastic contrast between the thin layer and the background media increases.

Inversion of V_p , V_s and density for thin layers with thickness between $\lambda/8$ and $\lambda/16$ using P wave data is possible using angles up to 50 degrees. For the PP-PS data, elastic parameters of these thin layers can be inverted using angles up to 40 degrees. For both cases, the uncertainty (especially the correlation between parameters) also becomes smaller as the elastic contrast between the thin layer and the background media increases.

In this paper, we analyzed a thin layer model with higher V_p , V_s and density than the background media; however, the same approach proposed here can be used to other thin layer models and other elastic parameters, such as impedance, Poisson ratio, and compressibility.

APPENDIX A

The reflectivity of an elastic thin layer

The term reflectivity refers to a generalized reflection coefficient that encompasses every event generated by the incidence of a plane harmonic wave on a layered elastic medium. Differently from a single interface reflection coefficient, a reflectivity is a frequency dependent function. The $r_{pp}^0(\omega)$ reflectivity responds to all ascendant P waves generated in the layered elastic medium as the result of incidence of a P wave, and the $r_{ps}^0(\omega)$ reflectivity responds to all ascendant S waves generated in the layered elastic medium as the result of an incidence of a P wave. These reflectivities can be obtained by a recursive matrix equation (Muller, 1985);

$$\mathbf{r}_{n-1}^B = \mathbf{R}_{n-1}^D + \mathbf{T}_{n-1}^U [\mathbf{I} - \mathbf{r}_n^T \mathbf{R}_{n-1}^U]^{-1} \mathbf{r}_n^T \mathbf{T}_{n-1}^D \quad (\text{A1})$$

where \mathbf{r}_n^B is the reflectivity matrix defined for the bottom of the n^{th} layer number;

$$\mathbf{r}_n^B = \begin{bmatrix} r_{pp}^n(\omega) & r_{sp}^n(\omega) \\ r_{ps}^n(\omega) & r_{ss}^n(\omega) \end{bmatrix} \quad (\text{A2})$$

The matrix $\mathbf{R}_n^{U,D}$ and $\mathbf{T}_n^{U,D}$ contains the upgoing and downgoing reflection and transmission coefficients for the interface at $z=z_n$;

$$\mathbf{R}_n^{U,D} = \begin{bmatrix} R_{pp}^{U,D} & R_{sp}^{U,D} \\ R_{ps}^{U,D} & R_{ss}^{U,D} \end{bmatrix}, \quad \mathbf{T}_n^{U,D} = \begin{bmatrix} T_{pp}^{U,D} & T_{sp}^{U,D} \\ T_{ps}^{U,D} & T_{ss}^{U,D} \end{bmatrix}.$$

These coefficients should be obtained through the solution of the Zoeppritz equation (see Aki & Richards for example). The symbol \mathbf{r}_n^T means the reflectivity matrix for the top of the n^{th} layer. The relationship between \mathbf{r}_n^T and \mathbf{r}_n^B is solely due to phase shifting and can be written as

$$\mathbf{r}_n^T = \mathbf{F}_n \mathbf{r}_n^B \mathbf{F}_n \quad (\text{A3})$$

where \mathbf{F}_n is the matrix that introduces the phase shift due the travel time of the waves in the n^{th} layer:

$$\mathbf{F}_n = \begin{bmatrix} e^{-ik_z^n h_n} & 0 \\ 0 & e^{-i\eta_z^n h_n} \end{bmatrix}. \quad (\text{A4})$$

The vertical wave numbers for P and S waves in the n^{th} layer are, respectively; $k_z^n = \omega \sqrt{(\frac{1}{\alpha_n})^2 - p^2}$ and $\eta_z^n = \omega \sqrt{(\frac{1}{\beta_n})^2 - p^2}$ and h_n is the thickness of the layer. Note that there is no upgoing waves in the last layer, so we can start the iteration with $\mathbf{r}_N^T = 0$, what implies, by means of (A1), that $\mathbf{r}_{N-1}^B = \mathbf{R}_{N-1}^D$. At each iteration of equation (A1), the transmission effects, internal multiples, and converted waves that occur in each layer are added to the solution until it reaches the top layer and the complete medium response will be contained in \mathbf{r}_0^B . For the single layer example presented in the main text (see Fig. 1), the reflectivity may be explicit given by:

$$\mathbf{r}_0^B = \mathbf{R}_0^D + \mathbf{T}_0^U [\mathbf{I} - \mathbf{F}_1 \mathbf{R}_1^D \mathbf{F}_1 \mathbf{R}_0^U]^{-1} \mathbf{F}_1 \mathbf{R}_1^D \mathbf{F}_1 \mathbf{T}_0^D \quad (\text{A5})$$

ACKNOWLEDGMENTS

The authors would like to thank Petrobras for supporting this work, through the research grant # 5850.0108361.18.9. This study has also been, in part, financed by the Coordenação de Aperfeiçoamento de Pessoal de Nível Superior (CAPES), through its graduate school support program, and by Conselho Nacional de Desenvolvimento Científico e Tecnológico (CNPq), through the Instituto Nacional de Ciência e Tecnologia Geofísica do Petróleo (INCT-GP).

REFERENCES

- AKI, K., & P. G. RICHARDS, 2002. Quantitative Seismology. University Science Books 2nd ed, ISBN-13: 978-1891389634. 700 pp.
- ASSIS, C. A. M., OLIVEIRA, S. A. M., MISSAGIA, R. M. & M. A. R. CEIA, 2017, Source wavelet and local wave propagation effects on the amplitude-variation-with-offset response of thin-layer models: A physical modeling study: *Geophysics*, 82(4), N27–N41, doi: 10.1190/geo2016-0262.1.
- BULAND, A. & OMRE, H., 2003, Bayesian wavelet estimation from seismic and well data: *Geophysics* 68 (6), doi: 10.1190/1.1635053. 2000-2009.
- DE HAAS, J.C. and BERKHOUT, A.J., 1988, On the Information Content of P-P, P-SV, SV-SV, and SV-P Reflections: SEG Technical Program Expanded Abstracts, 1190-1194, doi: 10.1190/1.1892487.
- DIEBOLD, J. B. & STOFFA, P. L., 1981, The travel time equation, tau- p mapping and inversion of common midpoint data: *Geophysics* 46(3), 238-254, doi: 10.1190/1.1441196.
- GELMAN, A., CARLIN, J. B., STERN, H. S., DUNSON, D. B., VEHTARI, A., RUBIN, D. B. 2013, Bayesian data analysis: Chapman & Hall / CRC Texts in Statistical Science, 3rd edition, ISBN-13: 978-1439840955. 675 pp.
- GOUVEIA, W. & J. A. SCALES, 1997, Resolution in seismic waveform inversion: Bayes vs. Occam: *Inverse Problems*, 13, 323-349, doi: 10.1088/0266-5611/13/2/009.
- GOUVEIA, W. & J. A. SCALES, 1998, Bayesian seismic waveform inversion: Parameter estimation and uncertainty analysis: *Journal of Geophysical Research*, 103, 2759-2779, doi: 10.1029/97JB02933.
- HASTINGS, W. K., 1970, Monte Carlo sampling methods using Markov chains and their applications: *Biometrika*, Oxford University Press (OUP), 57(1), 97-109.
- HILL, S. J., 2005, Inversion-based thickness determination: *The Leading Edge*, 24(5), 477-480, doi: 10.1190/1.1926799.
- HOUNIE, J. N. & OLIVEIRA S. A. M., 2014, The importance of locally converted waves on the elastic inversion of compressional data: *Brazilian Journal of Geophysics*, 32, 323-346, doi: 10.22564/rbpf.v32i2.462.
- JING, C. & RAPE, T., 2004, Resolvability analysis of rock property inversions of multicomponent seismic data: In: 74th Annual International Meeting, SEG Technical Program Expanded Abstracts, 897–900, doi: 10.1190/1.1845313. Denver, USA.
- KALLWEIT, R. S. & L. C. WOOD, 1982, The limits of resolution of zero-phase wavelets: *Geophysics*, 47(7), 1035–1046, doi: 10.1190/1.1441367.
- KHARE, V., & RAPE, T., 2007, Density inversion using joint PP/PS data: sensitivity to the angle range: In: 77th Annual International Meeting, SEG Expanded Abstracts, 965–969, doi: 10.1190/1.2792566. San Antonio, USA.
- KOEFOD, O., 1981, Aspects of vertical seismic resolution: *Geophysical Prospecting*, 29(1), 21-30, doi: 10.1111/j.1365-2478.1981.tb01008.x.
- LIU, Y., & SCHMITT, D. R., 2003, Amplitude and AVO responses of a single thin bed: *Geophysics*, 68(4), 1161–1168, doi: 10.1190/1.1598108.
- MALLICK, S., 2007, Amplitude-variation-with-offset, elastic-impedance, and wave-equation synthetics — A modeling study: *Geophysics*, 72(1), C1-C7, doi: 10.1190/1.2387108.
- METROPOLIS, N., ROSENBLUTH, A. W., ROSENBLUTH, M. N., TELLER, A. H. & TELLER, E., 1953, Equation of state calculations by fast computing machines: *The Journal of Chemical Physics*, AIP Publishing, 21(6), 1087–1092, doi: 10.1063/1.1699114.
- MÜLLER, G., 1985, Reflectivity method: A tutorial: *Journal of Geophysical Research*, 58, 153–174.
- OLIVEIRA, S. A. M., BRAGA, I. L. S., LACERDA, M. B., OUVENEY, G. F. & FRANCO, A. W. P., 2018, Extending the useful angle range for elastic inversion through the amplitude-versus-angle full-waveform inversion method, *Geophysics*, 83(3), R213-R226, doi: 10.1190/geo2017-0168.1.
- PAN, G. S., C. Y. YOUNG, & J. P. CASTAGNA, 1994, An integrated target-oriented prestack elastic waveform inversion: sensitivity, calibration, and application: *Geophysics*, 59(9), 1392—1404, doi: 10.1190/1.1443697.
- PENNA, R. & LUPINACCI, W., 2021, 3D modelling of flow units and petrophysical properties in Brazilian presalt carbonate: *Marine and Petroleum Geology*, 124, 104829. doi: 10.1016/j.marpetgeo.2020.104829.

- ROSA, A. L. R., & Ulrych, T. J., 1991, Processing via spectral modeling, *Geophysics*, 56(8), 1244-1251, doi: 10.1190/1.1443144.
- RUBINO, J. G. & VELIS, D., 2009, Thin-bed prestack spectral inversion. *Geophysics*, 74(4), R49-R57, doi: 10.1190/1.3148002.
- RUBINO, J. G. & VELIS, D. R., 2011, Seismic characterization of thin beds containing patchy carbon dioxide-brine distributions: A study based on numerical simulations: *Geophysics*, 76(3), R57-R67, doi: 10.1190/1.3556120
- SAMBRIDGE, M. & MOSEGAARD, K., 2002, Monte Carlo methods in geophysical inverse problems: *Reviews of Geophysics*, 40(3), 3-29, doi: 10.1029/2000RG000089.
- SIMMONS, J. L., & BACKUS M. M., 1994, AVO modeling and the locally converted shear wave: *Geophysics*, 59(8), 1237-1248, doi: 10.1190/1.1443681.
- TARANTOLA, A., 1987. *Inverse problem theory – methods for data fitting and model parameter estimation*. Elsevier Science Ltd., ISBN-13: 978-0444427656. 630 pp.
- VAN DER BAAN, M., 2008, Time-varying wavelet estimation and deconvolution by kurtosis maximization, *Geophysics*, 73(2), V11-V18, doi: 10.1190/1.2831936.
- VAN RIJSSSEN, E. P. F. & HERMAN G. C. , 1991, Resolution Analysis of Band-limited and Offset-limited Seismic Data for Plane-layered Subsurface Models: *Geophysical Prospecting*, 39(1), 61-76, doi: 10.1111/j.1365-2478.1991.tb00301.x..
- WIDESS, M. B., 1973, How thin is a thin bed? *Geophysics*, 38(6), 1176–1180, doi: 10.1190/1.1440403.
- WIDESS, M. B., 1982, Quantifying resolving power of seismic systems: *Geophysics*, 47(8), 1160–1173, doi: 10.1190/1.1441379.
- WIDMAIER, M. T., SHAPIRO, S. A. & HUBRAL, P., 1996, AVO correction for scalar waves in the case of a thinly layered reflector overburden: *Geophysics*, 61(2), 520-528, doi: 10.1190/1.1443978.
- ZENG, H., 2009, How thin is a thin bed? An alternative perspective: *The Leading Edge*, 28(10), 1192–1197, doi: 10.1190/1.3249773.

A.P.F. Development of methodology and computation of results; Writing of the manuscript; Generation of figures; Results analysis and discussion; **S.A.M.O.** Conception of the manuscript idea; Writing of the manuscript; Generation of figures; Results analysis and discussion; **F.S.M.** Theoretical background support; Writing of the manuscript; Results analysis and discussion.

Received on September 9, 2021 / Accepted on January 12, 2022